IEEE Access
Multidisciplinary | Rapid Review | Open Access Journal

Received March 13, 2022, accepted March 28, 2022, date of publication April 1, 2022, date of current version April 8, 2022.

Digital Object Identifier 10.1109/ACCESS.2022.3164072

Design and Characterization of Modified Comb Patch Antennas

ELENA MARONGIU[1], ALESSANDRO FANTI[1], (Member, IEEE), SANTI CONCETTO PAVONE[2], (Senior Member, IEEE), MATTEO BRUNO LODI[1], (Graduate Student Member, IEEE), ANDREA MELIS[1], NICOLA CURRELI[3], CLAUDIA MUSU[1], GINO SORBELLO[2], AND GIUSEPPE MAZZARELLA[1], (Senior Member, IEEE)

[1]Department of Electrical and Electronic Engineering (DIEE), University of Cagliari, 09123 Cagliari, Italy
[2]Department of Electrical, Electronics, and Computer Engineering (DIEEI), University of Catania, 95125 Catania, Italy
[3]Functional Nanosystems, Istituto Italiano di Tecnologia, 16163 Genova, Italy

Corresponding author: Alessandro Fanti (alessandro.fanti@unica.it)

This work was supported in part by the project "IQSS—Information Quality Aware and Secure Sensor Networks for Smart Cities," funded by Fondazione di Sardegna, within the three-year agreement between Fondazione di Sardegna and Sardininan universities (Regione Sardegna L.R. 7/2007, 2018, DGR 28/21–17.05.2015, CUP: F75F21001400007), and in part by the project "Ingegnerizzazione e Automazione del Processo di Produzione Tradizionale del Pane Carasau mediante di tecnologie IoT (IAPC)," funded by the Ministero dello Sviluppo Economico, in AGRIFOOD PON I&C 2014-2020 (CUP: B21B19000640008 COR: 1406652). The work of Santi Concetto Pavone was supported by the PON Research and Innovation Attraction and Mobility of Researchers (AIM) Project, Action I.2, granted by the FSE European Union Program. Santi C. Pavone wishes to thank also the project "PIACERI Quota 2D", granted by the Department of Electrical, Electronics and Computer Engineering of the University of Catania.

ABSTRACT This work deals with the proposal of a novel type of microstrip antenna, called MCPA the modified comb patch antenna. The proposed antennas is composed of *n* parallel conductors, fed by a common microstrip. A dedicated mathematical framework, based on the multiconductors transmission line formalism, is proposed for antenna analysis and design. The analytical model is numerically validated with full-wave simulations, resulting in a 5% error in the predicted resonant patch length. A numerical study of antenna matching, size, radiation performance is carried out. The matching increases as the number of conductors increases, whilst gain of comb antennas made of *n* conductors are about half dB higher than the equivalent full patch counterpart. Then, an eighty conductors was realized and measured to assess the frequency response of the antenna, as well as its radiation performances. An error of 1% between the predicted and measured value resonance frequency was observed. A difference of about 0.67 dB was found for the measured maximum antenna gain, with respect to the simulated one. The proposed antenna design is appealing for printed electronics and wearable, on-textile applications.

INDEX TERMS Comb antenna, multi-conductor, wireless body area network.

I. INTRODUCTION

The research interest in on-body wireless communication systems in recent years, is increasing due to the ever-growing relevance of personal electronic devices in everyday life and activities, such as personal communication [1], healthcare [2], identification, tracking and monitoring [3] of biometrics and biomedical parameters [4], [5]. In this framework, the electromagnetic engineering community is facing the challenge of designing and realizing innovative and low-cost antennas, which can be easily integrated in body area networks (BAN), or worn and integrated into wearable systems [6]. For these applications, microstrip antennas (e.g., patch) are mostly used, thanks to advantages such as ease of construction, low cost and a high adaptability. From an electromagnetic point of view, standard microstrip antennas have the relevant drawbacks of exhibiting low gain, reduced power capability and inherently narrowband [7]. To improve the performances of microstrp antennas, a pivotal requirement is to investigate new solutions, such as the use of multi-conductor antennas [8] or antenna arrays [9]. In this work, we propose a novel multi-conductor antenna. Therefore, when a new configuration is proposed, a robust, reliable and fast methodology for the study and optimization must be developed.

The associate editor coordinating the review of this manuscript and approving it for publication was Tutku Karacolak.

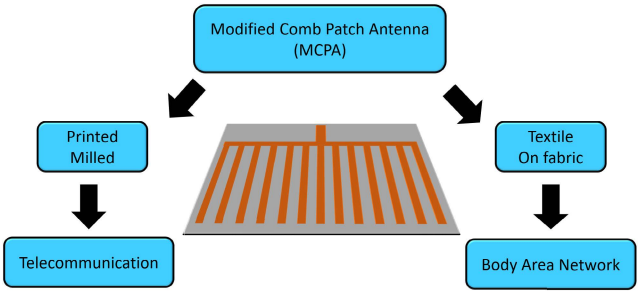

FIGURE 1. Concept, possible manufacturing approach and potential applications of the modified comb patch antenna MPCA.

This work proposes a modified comb patch antenna (MCPA), i.e. a patch composed of n parallel conductors, fed by a common microstrip line, as shown in Fig. 1. The conductors branch out from the feeding line perpendicularly in one direction, being symmetric with respect to the feeding line. The configuration is proposed to ensure that all the conductors are all placed along a given direction, thus determining a uniform current density flowing along with them. In addition, these requirements guarantee that the antenna characteristic parameters could be derived easily and efficiently, while providing a pure polarization of the antenna.

Fig. 2 shows the novel configuration proposed. The MCPA is an antenna topology which strongly differs from previous microstrip comb antennas. Indeed, the most commonly investigated, designed and characterized multi-conductor antenna are comb antennas, having conductors branching out in to opposite directions from a common microstrip feeding line or with a scope of 30° or 45° angle with respect to the feeding line [10]–[12]. Recently, a comb-shaped microstrip patch Antenna (CSMPA) was proposed [13]. Flexible broadband monopoles in comb arrangement, working in the frequency range 1.7-2.68 GHz, were studied [14]. The size of the lateral conductors leads to an increase in bandwidth (BW) (up to a 44.75% BW at −10 dB) and allows to slightly reduce the size of the antenna. The comb geometry has also been used for the

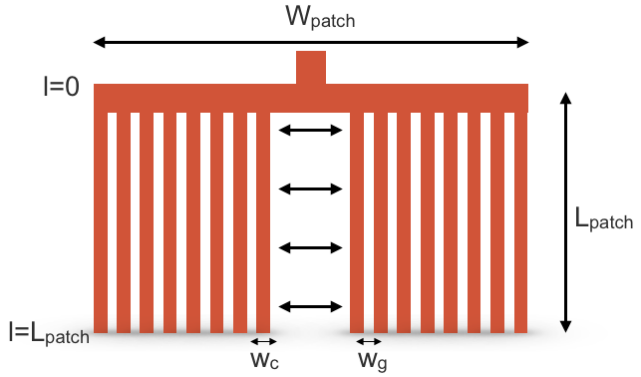

FIGURE 2. Geometry of a multi-conductor patch antenna. The feed is a 50 Ω microstrip line and the conductors are parallel microstrip segments having width w_c, spaced of w_g, with a length L_{patch}, the current flows uniformly along I in the z-direction.

design of arrays working at 2.45 GHz, reaching a maximum gain of 12.85 dB [15]. Comb antennas are mainly design in microstrip tecnology, or developed as a planar inverted F antenna (PIFA) for the applications in the UHF band [10]. Furthermore, metasurface structures can be obtained with linear multi-conductors [18]. Aslo, single and double side comb antennas for radar applications were proposed [19]. In [20], an EBG comb structure was proposed for enhancing the performance of antennas in WiMax band. A summary of the main literature about comb antennas is provided in Tab. 1.

TABLE 1. Resume of the state of the art of comb antennas.

Comb-shaped Antennas	Gain (dB)	Frequency (GHz)	$\|S_{11}\|$ (dB)
Comb array [15]	12.85	2.4	-34.88
PIFA [16]	1.3 dBi	0.915	-20
Linear array [17]	-	28	-24
Monopole [14]	-	2.15	-48
Metasurface [18]	5 dBi	28 - 56	< -10
Single comb [19]	6.05	5	-30
EBG structure [20]	-	2.65 - 7	-20

To summarize, the MPCA differs from previous comb antennas in the spatial arrangement of conductors. However, the difference between the proposed MCPA and the designs available in the literature is also the feeding strategy. Indeed, the use of a coaxial probe is the most used approach [14], [21]. The coaxial feed can present drawbacks from the design point of view and increases the technological criticalities for BAN applications (Fig. 1). The selection of the insertion point must be performed to ensure a homogeneous current flow in a single direction, thus raising difficulties in the design and matching procedures, hence calling for effective design strategies [10]–[14], [18]–[20]. Indeed, the traditional methods used for the design of microstrip patch antennas are not suitable for comb-shaped antennas. In this framework, comb antennas have been analyzed by developing models based on variational methods [22], modal analysis [23], or simple, but less accurate transmission line models (TLM) [24]–[26] or computationally costly, high-fidelity full-wave analysis (FW) [8], [27]–[33]. All these design strategies are often complemented by numerical optimization, heuristic or machine learning-based methods [34]–[38]. As a matter of fact, when designing the aforementioned comb antennas usually, the design strategy is mostly heuristic and driven by extensive numerical simulations [21], reflecting a poor theoretical effort [11], [13], thus highlighting the lack of a complete, exhaustive and simple model for the analysis of comb antennas. Therefore, there is a knowledge gap to be filed with a thorough and robust electroagnetics and antenna engineering analysis.

To the best of the authors' knowledge, the potentialities of this kind of MCPA, multi-conductor structure, have never been investigated. Therefore, in this work, a specific, original mathematical framework for designing the MCPA, of the type shown in Fig. 2, is developed. The proposed MCPA has the advantage of being cost-effective solution for communications and BAN applications. Furthermore, with the proposed

structure and the developed mathematical framework, the control on the intrinsic parasitic and matching capacitance makes this structure very flexible to be tuned.

The MCPA, shown in Fig. 2, is analyzed with a dedicated mathematical model aimed at the computation of the patch dimensions, to be matched and tuned in a given frequency range. The mutual coupling effects between the conductors, and the influence of the gaps are included in the thus allowing a realistic analytic model. The proposed model could be used to analyze and design MCPA printed or textile-based antennas (Fig. 1). The model is validated against numerical, full-wave simulations and experimental measurements. In this work, the selected frequency range is the GSM band (890-915 MHz). The proposed design and methodology is general and can be extended to other bands.

The paper is organized as follows, in Sect. II the set of equations for the design is presented. In Sect. III, both numerical and experimental validation are provided; then, in Sect. IV, the findings are presented and finally in Sect. V conclusion and discussion are given.

II. THE MODEL

The novel MCPA, shown in Fig. 2, can be analyzed as an n conductor transmission line system, supporting quasi-TEM modes [39], since the current flows uniformly along the l-direction. By applying the transmission line equations [Eq. (22) in the Appendix], the spatial variation of the voltage and current vectors ($1 \times n$) can be calculated. The equations must be manipulated to include the patch length (L_{patch}) in the expression for deriving the mathematical framework for design and analysis. With straightforward algebraic derivation, the coupled telegraphers' equations in the following second-order equation [40]

$$-\frac{d^2\underline{I}(l)}{d^2l} + \beta_0^2 \underline{\underline{L_n}}\,\underline{\underline{C_n}}\,\underline{I}(l) = 0 \tag{1}$$

for the k-th conductor, the solution to the second-order differential equation is in the following form

$$\underline{I}(l) = \underline{I}_k e^{j\beta_k l} \tag{2}$$

where β_k are the eigenvalues of the matrix $\beta_0^2 \underline{\underline{L_n}}\,\underline{\underline{C_n}}$ (with $k = 1, \ldots, n$). $\underline{\underline{L}}$ and $\underline{\underline{C}}$ are, respectively, the static, normalized inductance and capacitance matrices of the structure shown in Fig. 2. In other words, $\underline{\underline{C_n}} = \frac{1}{\epsilon_0} \cdot \underline{\underline{C}}$ and $\underline{\underline{L_n}} = \frac{1}{\mu_0} \cdot \underline{\underline{L}}$, respectively, being $\underline{\underline{C}}$ and $\underline{\underline{L}}$ the capacitances and inductances of the system, whilst ϵ_0 is the vacuum permittivity, in (Fm^{-1}) and μ_0 is the vacuum magnetic permeability, in (Hm^{-1}). In this case, it follows that, the propagation constant can be written as

$$\beta_k = \beta_0 \sqrt{\lambda_k} \tag{3}$$

where λ_k are the eigenvalues of the matrix $\underline{\underline{L_n}}$ and $\underline{\underline{C_n}}$, with size $n \times x\, n$. The term I_k indicates the eigenvector corresponding to the eigenvalue λ_k.

Then by rewriting the current in the form of a steady waves, we can impose the known current value for $l = L_{patch}$ and find that the voltage and current distribution as

$$\begin{cases} \underline{I}(l) = \sum_{k=1}^{n} \Big\{ \cos\left(\beta_0 \sqrt{\lambda_k}(l - L_{patch})\right) \cdot [I_{Ak}(L_{patch})] \\ \qquad + j \sin\left(\beta_0 \sqrt{\lambda_k}(l - L_{patch})\right) \cdot [B_k] \Big\} \underline{I}_k \\ \underline{V}(l) = j \frac{1}{\epsilon_0} \underline{\underline{C}}_n^{-1} \sum_{k=1}^{n} \Big\{ \cos\left(\beta_0 \sqrt{\lambda_k}(l - L_{patch})\right) \\ \cdot [I_{Ak}(L_{patch})] \\ \qquad + j \sin\left(\beta_0 \sqrt{\lambda_k}(l - L_{patch})\right) \cdot [B_k] \Big\} \underline{I}_k \end{cases} \tag{4}$$

where $I_k^+ + I_k^- = I_{Ak}(L_{patch})$ and $I_k^- - I_k^+ = B_k$, being I_k^+ and I_k^- unknown complex amplitudes.

Eqs. (4) are essential for deriving a procedure suitable for sizing the modified comb patch antenna, i.e. to find the values of W_{patch} and L_{patch} for the desired working frequency. To this aim, it is necessary to know the system capacitance and to further investigate the MCPA characteristic impedance.

A. DERIVATION OF L AND C PARAMETERS

In order to solve system (4) have to be derived the characteristic parameters $\underline{\underline{L}}$ and $\underline{\underline{C}}$ (see Fig. 2). The n conductors are placed between air and a dielectric substrate. Firstly the computation of the inductances in the MCPA is required. Indeed, the evaluation of the inductance in the system is straightforward once $\underline{\underline{C}}$ is known [41]: $\underline{\underline{L}}$ can be derived as the inverse of $\underline{\underline{C}}$ in air. Therefore, the capacitance matrix is derived from the total electric energy (W) stored in the structure, by a FD computational method [42]

$$C = \int_0^{L_{patch}} \int_0^{W_{patch}} \epsilon |\underline{E}|^2 \, dS \tag{5}$$

where ϵ is the dielectric permittivity of the medium and E is the electric field (Vm^{-1}).

To find the capacitance matrix of the system of n conductors, in this work, the calculation is performed for semplicity moving from the analysis of a four-conductor structure. Only explicit structures with equal strips, equal external gaps, and internal gaps equal or different to external gaps were considered (with reference to Fig. 3(a)), while taking into account the mutual-coupling between the MCPA elements.

Once the energy W is evaluated with the FD method, as previously described, it is found that,

$$W_k = \frac{1}{2} [\underline{v_k}]^T [C] [\underline{v_k}] \tag{6}$$

with v_k the chosen voltage vector and C is the capacity matrix [The Eq. (39) in the Appendix]. The Eq. (6) is a linear system of equations. Since it has six unknowns capacities, it requires six configurations. Therefore, we write a linear system of six equations in the six unknown capacities

$$\underline{\underline{A}} \cdot \underline{C} = \underline{W} \tag{7}$$

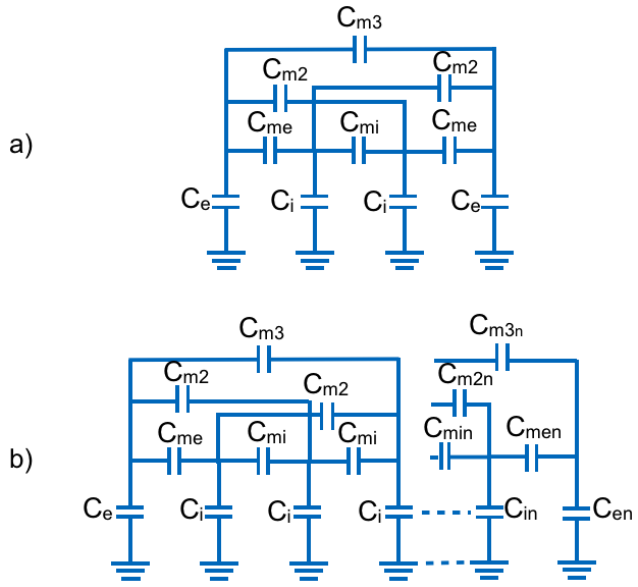

FIGURE 3. a) Circuital equivalent of the capacitive coupling between the four-conductors. b) Circuital equivalent of the capacitive coupling between the n-conductors.

where $\underline{\underline{A}}$ is the matrix which has as columns the six independent voltage (eigen-)vectors (v_k, with $k = 1, ..6$). By using the *Symbolic Toolbox* of Matlab 2019b (The MathWork Inc., MA, USA) it is possible to derive a set of eigen-vectors which ensures that $\underline{\underline{A}}$ is well conditioned and symmetric. It is worth to point out that two of the eigenvectors terms are known, whilst the other two are symmetrical. The values of the four-line structure were then used as an approximation to obtain the matrix $\underline{\underline{C}}$ of a n-conductors system Fig. 3(b). The internal capacitances were approximated by the value of C_i of the 4-conductors, and all mutual internal capacitances were approximated with C_{mi}, C_{m2} and C_{m3}. Similarly, the two external capacitances were approximated with C_e, and the two mutual external capacitances were approximated by C_{me}. Therefore, the final matrix, for the n-conductor system is

B. MODEL FOR MCPA DESIGN

We have presented the computation of the transmission line parameters for studying the modified comb patch antenna in its fingers (Fig. 2). However, to study the system as an antenna, the input impedance is fundamental to derive exactly how to design the device for working under resonance conditions and match the system to the feeding line. Therefore, the input impedance can be found using the voltage and current equations of the system (4), and then a suitable design strategy can be derived. As a result, an objective of the proposed model is the calculation of the radiation impedance considering the couling effects for adjacent conductors, thus introducing additional complexity.

As first step, at the transverse line from which the set of parallel conductors branch out (see Fig. 2) all the k-th tensions must be equal, i.e.

$$V(0) = \begin{bmatrix} 1 \\ 1 \\ \vdots \\ 1 \end{bmatrix}_{1n} \cdot V_g \tag{8}$$

where V_g is the supply voltage. For $l = 0$ Eqs. (4) can be written as

$$1 \cdot V_g = \frac{1}{j\omega\epsilon_0} \underline{\underline{C_n}}^{-1} \sum_{k=1}^{n} \underline{I}_{Ak}(L_{patch})\beta_0\sqrt{\underline{\lambda}_k} \cdot \sin(\beta_0\sqrt{\underline{\lambda}_k}L_{patch}) + jB\sqrt{\underline{\lambda}_k}\cos(\beta_0\sqrt{\underline{\lambda}_k})\underline{I}_k \tag{9}$$

where $B = B_k\beta_0$.

The voltage in $l = L_{patch}$ is instead expressed as

$$\underline{V}(L_{patch}) = \underline{\underline{Z}}_{irr} \cdot \underline{I}(L_{patch}) \tag{10}$$

where $\underline{\underline{Z}}_{irr}$ is the radiation impedance matrix and L_{patch} is an unknown.

If the coupling between the set of parallel conductors is neglected, the matrix $\underline{\underline{Z}}_{irr}$, or the admittance matrix, is diagonal, with real input resistances, related to the single conductor [43]. In other words, in absence of coupling, $\underline{\underline{Z}}_{irr}$ is equal to

$$\underline{\underline{Z}}_{irr} = \text{diag}(R_n) \tag{11}$$

where R_n is the resistance of the single n-th conductor (assumed to be all equal), i.e. $R_n = 90n(\frac{\lambda_0}{w_c})^2$.

$$C_n = \begin{bmatrix} C_{11} & 0 & \dots & 0 \\ 0 & C_{22} & \dots & 0 \\ \vdots & & & \\ 0 & \dots & C_{33} & 0 \\ 0 & \dots & 0 & C_{44} \end{bmatrix} \tag{12}$$

When the coupling between conductors is neglected, the real-valued impedance matrix can be used to find the resonant L_{patch} value. However, the operation under this assumption would lead to over/underestimated results. Therefore, in this work, a more in-depth analysis is performed.

Under the approximation of neglecting the coupling between the conductors, the results are limiting and less accurate for the analysis and design of the MCPA. Therefore, the proposed mathematical framework for the MCPA can be complicated by accounting for the coupling between conductors in the evaluation of the irradiation admittance. It is worth highlighting that, in this work, the radiation impedance is not calculated using the classic formula described by Eq. (11), but, instead, it is computed by comparing the total avaialable power with the radiated field. Therefore, he radiation admittance Y_{irr} is a full, complex matrix which accounts for the coupling between all conductors. Hence, the total power in the system can be written as follows [44], [45]

$$P_c = \frac{1}{2}V_n^T Y V_n^* = \sum_{p,m=1}^{n} V_{n,p}V_{n,m}^* Y_{p,m}^* \tag{13}$$

where V_n is the voltage on the single conductor.

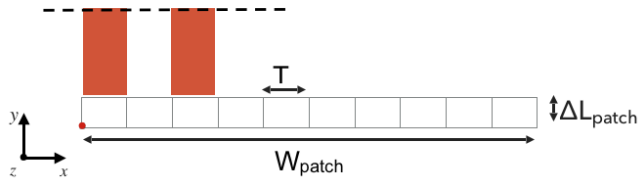

FIGURE 4. Configuration and discretization of the electric field in the multi-conductor system for computing the total power accounting for the coupling. The coordinate system is different from Fig. 2. The red dot indicates the starting point of x_p and x_m.

The electric field can be written as a piecewise constant function, as shown in Fig. 4, in the MCPA system, for n lines, having width $T = \frac{W}{n}$ and with $x_p = pT$, $x_m = mT$. Therefore, to ease the analytical derivation, we can perform the Fourier transform of the electric field and get

$$\begin{aligned}\widetilde{\underline{E}} &= \hat{i}_y T \sum_{p=1}^{n} V_{n,p} \mathrm{sinc}\Big(\frac{T}{2}k_x\Big)\mathrm{sinc}\Big(\frac{\Delta l}{2}k_y\Big)e^{ik_x x_p} \\ \widetilde{\underline{E}}^* &= \hat{i}_y T \sum_{p=1}^{n} V^*_{n,m} \mathrm{sinc}\Big(\frac{T}{2}k_x\Big)\mathrm{sinc}\Big(\frac{\Delta l}{2}k_y\Big)e^{-ik_x x_m} \end{aligned} \quad (14)$$

where $\hat{i_y}$ is the unit vector along the y-direction, as shown in Fig. 4, and k_x and k_y are the componetns of the propagation vectors along $\hat{i}_x$ and $\hat{i}_y$. Hence, by using Eq. (14), we can rewrite Eq. (13) as

$$P_C = \frac{1}{8\pi^2 k\eta}\iint_{-\infty}^{+\infty}\Big\{k_z^2|\widetilde{\underline{E}}|^2 + |k_y\widetilde{\underline{E}}|^2\Big\}\frac{dk_x dk_y}{k_z^*} \quad (15)$$

Where η is the free-space intrinsic impedance. To derive $|\widetilde{\underline{E}}|^2$, we multiply Eq. (14) together

$$\begin{aligned}|\widetilde{\underline{E}}|^2 &= T^2\mathrm{sinc}\Big(\frac{T}{2}k_x\Big)\mathrm{sinc}\Big(\Delta l^2 k_y\Big)\sum_{p=1}^{n} V_{n,p}V^*_{n,m}e^{ik_x x_d} \\ &= M(k_x,k_y)\sum_{p=1}^{n} V_{n,p}V^*_{n,m}e^{ik_x x_d} \end{aligned} \quad (16)$$

where $x_d = x_p - x_m$; Wheres $M(k_x, k_y)$ is defined as

$$M(k_x,k_y) = \mathrm{sinc}\Big(\frac{T}{2}k_x\Big)\mathrm{sinc}\Big(\Delta l^2 k_y\Big) \quad (17)$$

That is the spectrum of a 2D constant truncared spatial function (Fig. 4).

Finally, by substituting (16) into (15), we find

$$\begin{aligned}P_C = \frac{1}{8\pi^2 k\eta}\iint_{-\infty}^{+\infty}\Big\{k_z^2 + |k_y|^2\Big\}\Big\{\cos k_x(x_d) + \\ -j\sin k_x(x_p - x_m)\Big\}\frac{dk_x dk_y}{k_z^*}\end{aligned} \quad (18)$$

Finally, by comparing (13) and (18), we can find the complex admittance of the MCPA antennas as

$$\begin{aligned}Y^*_{p,m} = \frac{1}{4\pi^2 k\eta}\iint_{-\infty}^{+\infty}\Big\{k_z^2 + |k_y|^2\Big\}M(k_x,k_y) \\ \times\Big\{\cos k_x(x_d) - j\sin k_x(x_p - x_m)\Big\}\frac{dk_x dk_y}{k_z^*}\end{aligned} \quad (19)$$

As detailed in the Appendix, by manipulating Eq. (19), the radiation admittance can be divided into real and imaginary part to get the closed form expression for both the real part, so that

$$\begin{aligned}R_e\{Y^*_{p,m}\} = \frac{T^2}{\pi^2 k\eta}\int_0^k (k^2 - k_y^2)M(k_x,k_y)\cdot \\ \frac{\pi}{(k^2-k_x^2)\Delta l^2}\sum_{0}^{+\infty}\frac{(-1)^n\Delta l(k^2-k_x^2)^{2n+1}}{(2n+2)(2n+1)2^{2n}(n!)^2} \\ \cdot\cos k_x(x_d)dk_x\end{aligned} \quad (20)$$

The imaginary part of the admittance is also found in closed-form by using the Rhodes' relationships (see Appendix for details) [46]

$$\begin{aligned}I_m\{Y^*_{p,m}\} = \frac{T^2}{\pi^2 k\eta}\int_0^k (k^2 - k_y^2)\mathrm{sinc}\Big(\frac{T}{2}k_x\Big) \\ \times\cos k_x(x_d)\Big\{\int_{\sqrt{k^2-k_x^2}}^{-\infty}\mathrm{sinc}^2\Big(\frac{\Delta l}{2}k_y\Big) \\ \times\frac{dk_x dk_y}{\sqrt{k^2-k_x^2-k_y^2}}\Big\}dk_x + \frac{T^2}{\pi^2 k\eta} \\ \times\int_k^{+\infty}(k^2-k_y^2)\mathrm{sinc}\Big(\frac{T}{2}k_x\Big)\cos k_x(x_d) \\ \times\Big\{\int_0^{+\infty}\mathrm{sinc}^2\Big(\frac{\Delta l}{2}k_y\Big)\frac{dk_x dk_y}{\sqrt{k^2-k_x^2-k_y^2}}\Big\}dk_x\end{aligned} \quad (21)$$

The analytical expressions for both real and imaginary parts of the total power is manipulated and solved by Mathematica v. 10.0 (Wolfram, GE). After having derived the closed-form expressions, the computation was carried out with Matlab *Symbolic Toolbox* and the impedance value of the single conductor element is found to fill the admittance matrix.

In order to design the MCPA antenna we need to find the set of length (L_{patch}) and width (W_{patch}) of the patch to work at the desired frequency range, under resonance conditions. To this aim, by imposing the imaginary part of the admittance to be zero and by using the bisection iterative method [47] the effective length of the patch which satisfies this condition can be found numerically.

III. VALIDATION

A. NUMERICAL VALIDATION

In order to validate if the proposed model is suitable for designing a MCPA antenna, we compare our Matlab code with numerical, full-wave simulations performed in CST (Simulia, 3DS, GE). As shown in Fig. 5, we considered two multi-conductor comb patch antennas with $n = 20$ and $n = 80$ conductors. The substrate is a RT/Duroid 5880 with thickness $h_{sub} = 1.5$ mm and nominal $\epsilon_r = 2.2$. The proposed design is also compared to the standard rectangular patch antenna,

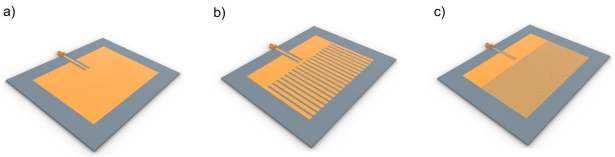

FIGURE 5. a) Rendered geometry of the reference patch. b) Rendered geometry of the 20 conductors comb patch antenna. c) Rendered geometry of the 80 conductors comb patch antenna.

as control and reference case, as shown in Fig. 5. The antennas are fed by a microstrip line connected to a 223-CON-SMA-EDGE-S. The sizes of the patches for the validation are reported in Tab. 2.

TABLE 2. Properties and geometries of the size of the reference patch and two MCPA. All dimensions are in millimeters.

Parameter	n = 20	n = 80	Full Patch
W_{patch} (mm)	150	150	131
L_{patch} (mm)	106.8	110.6	108.1
W_c (mm)	5	1.25	-
W_g (mm)	2.6	0.65	-
h_{sub} (mm)	1.575	1.575	1.575
L_{inset} (mm)	30	30	30

The frequency range used in the simulation is 800-1000 MHz. We used as figures of merits the MCPA antenna size ($L_{patch} \times W_{patch}$), the characteristic impedance and the return loss ($|S_{11}|$). With this further comparison, the pros and cons of the MCPA antenna performance are critically analyzed to gain further insight into the full exploitation of its potential for telecommunications or on-body applications.

B. PROTOYPE FABRICATION AND EXPERIMENTAL CHARACTERIZATION

After having analyzed the proposed antenna topology, we selected a case study to manufacture and characterize. The LPKF ProtoMat E44 (LPKF Laser & Electronics AG, GE) milling machine was used for manufacturing the $n = 80$ conductors MCPA.

The return loss of the MCPA was measured with Haelwtt-Packard 8720C vector network analyzer (VNA), as shown in Fig. 6. The antenna gain was measured with the three antenna method, by using the $n = 80$ conductors MCPA as antenna under test, together with the LP0410 PCB log-periodic directional antenna (National Instruments, with 5-6 dB of gain, working frequencies 400-1000 MHz) and the log-periodic USLP9142 (D-69250, Schwarzbeck, Schonau GE) antenna working between 800-1000 MHz, presenting a 3.7-6.8 dB gain [48]. The antennas were placed at a distance d_A of 3.3 m, being $d_A \gg 2 \cdot W_{patch}^2/\lambda$. The same VNA is used. The radiation patterns for $\phi = 0°$ and $\phi = 90°$ were acquired at 0°, 45°, 90°, 180° angles.

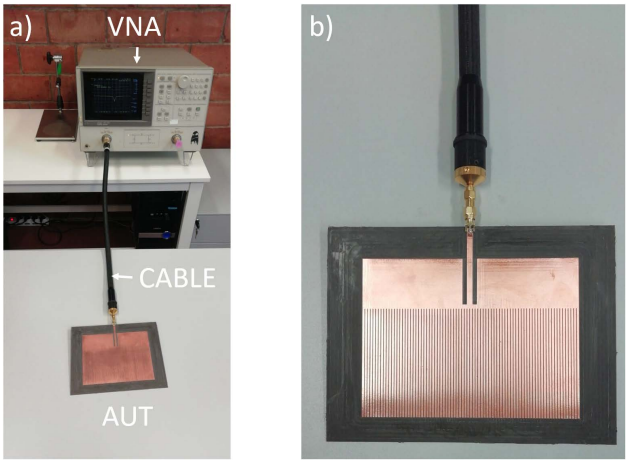

FIGURE 6. a) Experimental setup for the return loss ($|S_{11}|$) measurement. b) Magnified image of the milled multi-conductor patch antenna.

IV. RESULTS

A. MODEL VALIDATION & ANALYSIS

The parameters used in the numerical simulations of the reference patch and the MCPA with a variable number of conductors are reported in Tab. 2. We have compared the resonance length computed by the proposed mathematical framework and that obtained by empirical refinement on CST. The results are shown in Fig. 3. The values of the relative percentage error calculated assuming as reference the CST simulations are reported in Tab. 3. It can be noticed that the error increase as the number of conductors increases. Given that the width of the patch is constant, from the geometry shown in Fig. 2, the size of conductors decreases. Therefore, the width of each comb line and the size of the gap halves when the number of conductors is doubled. In this framework, the accuracy in the evaluation of the model parameters presents a reduction, which results in a fourfold error on the patch length. However, it must be noticed that the error, with respect to the ground through of the full-wave simulation, is below 5%, which can be considered as a valuable result.

TABLE 3. Comparison of the calculated lengths for the three different patches.

Patch	CST	Matlab	Error
n = 20	106.8 mm	105 mm	1.68%
n = 80	110.6 mm	115.02 mm	4.4%

Given the promising results, we have numerically investigated how the variation of the conductor numbers influences the antenna performances, in terms of matching, gain and directivity. The simulation results are reported in Tab. 4. The increase in n results in a non-linear variation of the patch length, up to the asymptotic limit of a classic, full patch, as shown in Fig. 7. On the other hand, the matching of the MCPA decreases in a hyperbolic way (see Tab. 4). We have compared this figure of merit by observing the $|S_{11}|$ vs.

TABLE 4. Comparison of antenna parameters for different number of conductors.

Conductors	$\|S_{11}\|$ (dB)	-10 dB BW (%)	Gain (dB)	Directivity (dB)	Efficiency (%)	L_{patch} (mm)
$N = 4$	-21.9	0.66	6.44	7.73	74	92.8
$N = 12$	-19.70	0.71	6.55	7.71	77	94
$N = 20$	-28.6	0.73	6.65	7.58	78	106.8
$N = 40$	-28.88	0.71	6.67	7.68	79.3	110
$N = 80$	-35.75	0.70	6.37	7.75	80	110.6
$N = 160$	-42.03	0.67	6.68	7.72	80	112
$N \to \infty$	-41.42	0.64	6.26	7.6	73	108.1

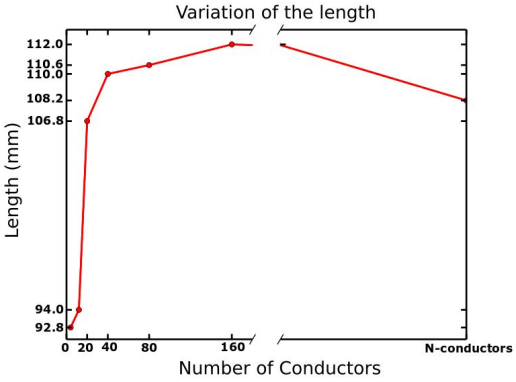

FIGURE 7. Simulated patch lengths (mm) as a function of conductor numbers (n).

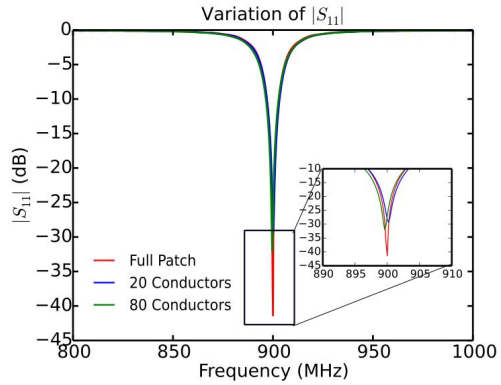

FIGURE 8. Comparison of simulated S_{11} parameter for the two MCPA and ther reference patch. Dimensions are shown in Tab. 2.

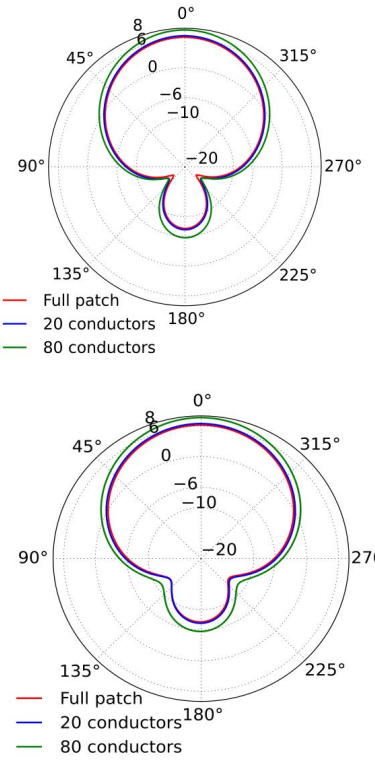

FIGURE 9. Simulation radiation pattern in yz-plane and xz-plane for the three antennas considered, where the dimensions are shown in Tab. 2.

frequency, as shown in Fig. 8. It can be noticed that the bandwidth of the MCPA increases by decreasing the number of conductors, as reported in Tab. 4. However, it must be noticed that, for a large n, the performances tends to that of a standard patch. From Tab. 4, it is possible to observe that the gain has a narrow variation with the n (i.e., about 0.42 dB). Remarkably, that the MCPA structure presents a simulated gain slightly higher than the reference patch antenna, as shown in Fig. 9. The same consideration holds for the directivity of the MCPA (Tab. 4). On the other hand, the antenna efficiency (in %), reported in Tab. 4 presents a larger variations (up to 2-7%) with n. This last finding is very relevant and show the promising character of the MCPA for future use.

B. EXPERIMENTAL CHARACTERIZATION

Among the designed MCPA, we selected the 80-conductors antenna as the best candidate for performing the experimental characterization. The tested prototype is shown in Fig. 6.b. The comparison of the measurements and the simulation results are reported in Fig. 10. From Fig. 10, we found a difference of 0.7% between the simulations and the measured performances, guaranteeing for the prototype a -10 dB BW of 1%. The resonance of the realized MCPA occurs at 910.25 MHz, instead of 901.3 MHz, with a 1.1% difference from the simulated value. To demonstrate that the frequency shift is not due to an error in the proposed mathematical model for the MCPA design, we performed an additional numerical simulation to elucidate the fact that the substrate batch used threin presented a large variability from the nominal value of the dielectric permittivity ($\epsilon_r = 2.2$). Therefore, in Fig. 10, the simulated $|S_{11}|$ for the MCPA with 80 conductors varying ϵ_r from 2.08 to 2.34, according to the variability

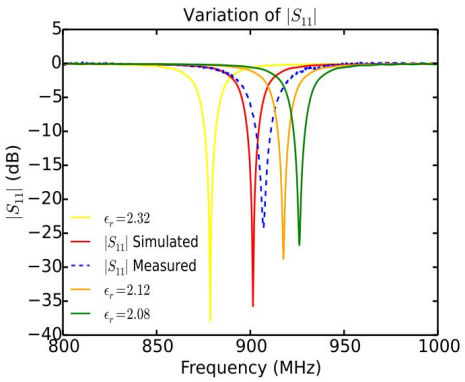

FIGURE 10. Comparison between the simulated curves and measured $|S_{11}|$ data of a modified comb patch antenna with 80 conductors by varying the dielectric permittivity of the Rogers substrates.

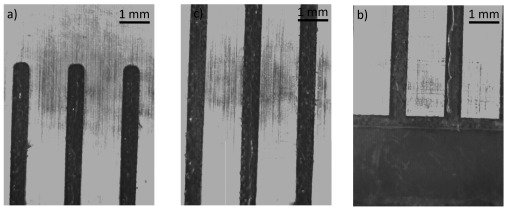

FIGURE 11. a) Optical image of the manufactured MPCA nearby the feeding line, at the conductor branches. b) Magnification of the multiconductor structure. c) Detail of the termination of the MPCA.

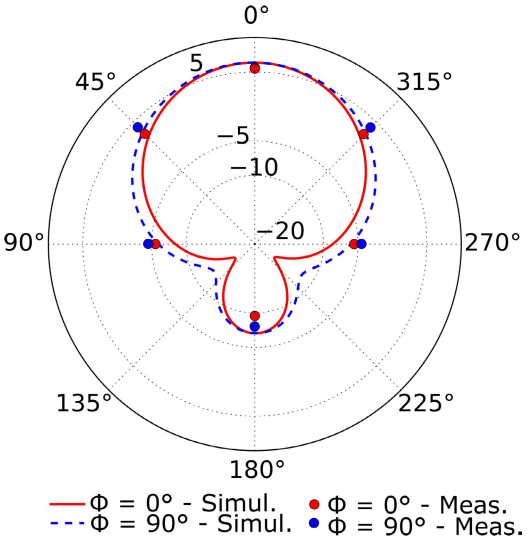

FIGURE 12. Measured vs. simulated radiation pattern of the modified comb patch antenna for $n = 80$ conductors.

reported in the datasheet. By comparing the measured return loss shown in Fig. 10 and the curves in Fig. 10, we can noticed that the actual relative dielectric permittivity of the substrate is 2.12. These findings are supported by the analysis of the manufactured antenna geometry, whose geometric features are respected well within the mechanical tolerances admissible in the GSM band, as shown in Fig. 11. Finally, the radiation performances of the manufactured MPCA were measured and the findings, for comparison with the simulations, are reported in Fig. 12. The measured maximum antenna gain is 5.75 dB, which differs by ∼0.63 dB from the simulated one. For angles higher than 0°, the maximum difference between the measured value and the simulated one is about 1.75 dB.

These findings indicate that our model can effectively be used to design a modified comb patch antenna with satisfactory performances in terms of tuning, matching and radiation.

V. CONCLUSION AND DISCUSSIONS

This work dealt with the design, realization and characterization of modified comb patch antennas. We developed and provided design equations in closed-form for sizing a patch composed of n parallel conductors fed by a common microstrip line. By comparison with full-wave numerical simulations, we found that our model can predict the resonance length of the patch with a maximum error of 4.4%. The proposed topology is a novel arrangement and present the advantage of adding degrees of freedom for tuning the antenna performances. We investigated numerically the effect of increasing the number of conductors on antenna behavior. We realized a prototype of a MCPA with 80 conductors and experimentally characterized its performances. Concerning predicted curves, a 1.1% shift in the resonance frequency was found. This effect can be ascribed to a 3.7% variation in the relative dielectric permittivity of the substrate.

Given that, compared to a standard patch antenna, the MPCA is low-cost, easy to manufacture, while presenting a reduced conductor area, it also demonstrated increased gain, slighlty larger bandwidth, enhanced radiation efficiency and larger directivity, it is appealing and of potential interest for innovative applications. In particular, the possibility of obtaining matching, tuning and radiation performances comparable (or even higher) than a standard patch while using a lower amount of conductor material could be relevant for realizing communication systems in a sustainable, cost-effective way through printed electronics manufacturing techniques [49]. Furthermore, the MCPA configuration is interesting for designing textile-based antennas. Indeed, the antenna design shown in Fig. 2 is very appealing for BAN since the MCPA can be an electronic device easily integrable in garments. Indeed, we forecast that the proposed MCPA can be implemented by usign conductive fibers in the arrangment shown in Fig. 1, ensuring good radiation performances in an on-body scenario. In fact, by using conductive textiles the MPCPA geometry could be easily weaved. To date, several examples of textile, wearable antennas were proposed, such as the woven textiles antennas from [50], the electro-textile antennas made up of a mix of metallic and fabric filaments [51], the RFID tag manufactured with a sewing machine directly on clothes [52] or antennas synthesized with hydrophobic materials were studied [53], [54]. However, the complexity of the embroidery thread of the aforementioned antennas does not allow to perform a rigorous analysis

(e.g., with TLM or FW approach) or an effective, easy and accurate design. The MCPA could be a cost-effective solution with a reasonable trade-off between performances and design complexity. Therefore, future works may deal with the design, realization and characterization of textile-based MCPA.

APPENDIX

A. DERIVATION OF MAIN EQUATIONS

The analysis and design equations of the MCPA are derived from the transmission lines equations:

$$\begin{aligned} -\frac{d\underline{V}(l)}{dl} &= j\omega\mu_0\underline{\underline{L_n}}\underline{I}(l) \\ -\frac{d\underline{I}(l)}{dl} &= j\omega\epsilon_0\underline{\underline{C_n}}\underline{V}(l) \end{aligned} \tag{22}$$

where the $\underline{\underline{L}}$ and $\underline{\underline{C}}$ are, respectively, the static, normalized inductance and capacitance matrix of the structure shown in Fig. 2. In other words, $\underline{\underline{C_n}} = \frac{1}{\epsilon_0} \cdot \underline{\underline{C}}$ and $\underline{\underline{L_n}} = \frac{1}{\mu_0} \cdot \underline{\underline{L}}$, respectively, being $\underline{\underline{C}}$ and $\underline{\underline{L}}$ the capacitances and inductances of the system, whilst ϵ_0 the vacuum permittivity, in Fm^{-1} and μ_0 the vacuum magnetic permeability, in Hm^{-1}. In the MCPA, the dielectric is not homogeneous, thus implying that quasi-TEM modes are supported [39]. Therefore, moving from the system (22), by taking the first derivative, with respect to the local space variable l, of the second equation of the system (22), we obtain,

$$-\frac{d^2\underline{I}(l)}{d^2l} = j\omega\epsilon_0\underline{\underline{C_n}}\frac{d\underline{V}(l)}{dl} \tag{23}$$

By substituting Eq. (22) in Eq. (23), we get:

$$-\frac{d^2\underline{I}(l)}{d^2l} + j\omega\epsilon_0\underline{\underline{C_n}}\,\underline{\underline{L_n}}\underline{I}(l) = 0 \tag{24}$$

Then, Eq. (24) can be written as follows:

$$-\frac{d^2\underline{I}(l)}{d^2l} + \beta^2\underline{I}(l) = 0 \tag{25}$$

By introducing the following relationships, where f is the working frequency and c_0 is the speed of light in vacuum,

$$\begin{cases} \sqrt{\epsilon_0\mu_0} = \dfrac{1}{c_0} \\ \omega = 2\pi f \\ \beta_0 = \dfrac{2\pi f}{c_0} \end{cases} \tag{26}$$

then Eq. (22) turns into,

$$\begin{cases} \underline{V}(l) = -\dfrac{1}{\omega\epsilon_0}\underline{\underline{C_n}}\dfrac{d\underline{I}(l)}{dl} \\ -\dfrac{d^2\underline{I}(l)}{d^2l} + \beta_0^2\underline{\underline{L_n}}\,\underline{\underline{C_n}}\underline{I}(l) = 0 \end{cases} \tag{27}$$

The solution to the second-order differential equation is in the following form:

$$\underline{I}(l) = \underline{I}_k e^{j\beta_k l} \tag{28}$$

where β_k are the eigenvalues of the matrix $\beta_0^2\underline{\underline{L_n}}\,\underline{\underline{C_n}}$ (with $k = 1, \ldots, n$). In this case, it follows that,

$$\beta_k = \beta_0\sqrt{\lambda_k} \tag{29}$$

where λ_k (with k ranging from 1 to n) are the eigenvalues of the matrix $\underline{\underline{L_n}}$ and $\underline{\underline{C_n}}$, with size $n \times n$, and the term $\underline{I}_k$ indicates the eigenvector corresponding to the eigenvalue λ_k.

Therefore, the current in the MCPA antenna can be written in the following form,

$$\underline{I}(l) = \sum_{k=1}^{n}(I_k^+ e^{-j\beta_k l} + I_k^- e^{j\beta_k l})\underline{I}_k \tag{30}$$

where I_k^+ and I_k^- are scalar with suitable values. Now, by expanding the exponential terms of the current, it follows,

$$\begin{cases} \underline{I}(l) = \displaystyle\sum_{k=1}^{n}\Big[I_k^+\cos(\beta_k l) - jI_k^+\sin(\beta_k l) \\ \qquad + jI_k^-\cos(\beta_k l) + jI_k^-\sin(\beta_k l)\Big]\underline{I}_k \\ \underline{V}(l) = j\underline{\underline{C_n}}^{-1}\displaystyle\sum_{k=1}^{N}\Big[I_k^+\cos(\beta_k l) - jI_k^+\sin(\beta_k l) \\ \qquad + jI_k^-\cos(\beta_k l) + jI_k^-\sin(\beta_k l)\Big]\underline{I}_k \end{cases} \tag{31}$$

If we group the sine and cosine terms, we get,

$$\underline{I}(l) = \sum_{k=1}^{n}[\cos(\beta_k l)(I_k^+ + I_k^-) + j\sin(\beta_k l)(I_k^- - I_k^+)]\underline{I}_k \tag{32}$$

By knowing the voltage and current in $l = L_{patch}$, shown in Fig. 2, we can write:

$$\begin{aligned} \underline{I}(l) = \sum_{k=1}^{n}\Big\{&\cos(\beta_0\sqrt{\lambda_k}(l - L_{patch}))\cdot[I_{Ak}(L_{patch})] \\ &+ j\sin(\beta_0\sqrt{\lambda_k}(l - L_{patch}))\cdot[\beta_k]\Big\}\underline{I}_k \end{aligned} \tag{33}$$

where,

$$I_k^+ + I_k^- = I_{Ak}(L_{patch}) \tag{34}$$

$$I_k^- - I_k^+ = B_k \tag{35}$$

Eq. (31) can be re-written in the steady form (for the k-th eigenvalue and the n-th conductor, i.e.,

$$\begin{cases} \underline{I}(l) = \displaystyle\sum_{k=1}^{n}\Big\{\cos(\beta_0\sqrt{\lambda_k}(l - L_{patch}))\cdot[I_{Ak}(L_{patch})] \\ \qquad + j\sin(\beta_0\sqrt{\lambda_k}(l - L_{patch}))\cdot[B_k]\Big\}\underline{I}_k \\ \underline{V}(l) = j\dfrac{1}{\epsilon_0}C_n^{-1}\displaystyle\sum_{k=1}^{n}\Big\{\cos(\beta_0\sqrt{\lambda_k}(l - L_{patch})) \\ \cdot[I_{Ak}(L_{patch})] \\ \qquad + j\sin(\beta_0\sqrt{\lambda_k}(l - L_{patch}))\cdot[B_k]\Big\}\underline{I}_k \end{cases} \tag{36}$$

B. CAPACITANCE CALCULATION

1) CAPACITY MATRIX REPRESENTATION

The basic structure considered for the calculation of the capacities consists of four conductors. The matrix of the capacities found for four conductors consists of six elements, these six elements or describe the external, internal and mutual capacities between the conductors. The capacity matrix can be constructed as a block matrix, composed of four blocks defined as follows:

$$C_1 = \begin{bmatrix} C_e + C_{me} + C_{m2} + C_{m3} & -C_{me} \\ -C_{me} & C_i + C_{me} + C_{mi} + C_{m2} \end{bmatrix} \tag{37}$$

$$C_2 = \begin{bmatrix} -C_{m2} & -C_{mi} \\ -C_{m3} & -C_{m2} \end{bmatrix}, C_3 = \begin{bmatrix} -C_{m2} & -C_{m3} \\ -C_{mi} & -C_{m2} \end{bmatrix} \tag{38}$$

Being a diagonal matrix, the blocks C_4 a are equivalent to the block C_1 with the elements of the diagonal reversed.

$$C = \begin{bmatrix} C_1 & C_2 \\ C_3 & C_4 \end{bmatrix} \tag{39}$$

The structure with four conductors can be generalized to a structure with n conductors. In this case the matrix C can be written as:

$$C_n = \begin{bmatrix} C_{11} & 0 & \dots & 0 \\ 0 & C_{22} & \dots & 0 \\ \vdots & \dots & C_{33} & 0 \\ 0 & \dots & 0 & C_{44} \end{bmatrix} \tag{40}$$

2) COMPLETE DERIVATION OF REAL AND COMPLEX IMPEDANCES OF THE MCPA ANTENNA

When the coupling between conductors is taken into account, the system admittance is a complex, dense matrix. To design the MCPA antenna, the length (L) and width (W) of the patch can be found numerically by imposing the imaginary part of the Eq. (19) to be equal to zero. Moving from Eq. (19), the two exponential contribution of the integrals can be highlighted,

$$\begin{aligned} Y^*_{p,m} = {} & \frac{1}{4\pi^2 k\eta} \iint_{-\infty}^{+\infty} \left\{k_z^2 + |k_y|^2\right\} M(k_x, k_y) \\ & \times \left\{ \cos k_x (x_p - x_m) \right\} \frac{dk_x dk_y}{k_z^*} \\ & -j \frac{1}{4\pi^2 k\eta} \iint_{-\infty}^{+\infty} \left\{k_z^2 + |k_y|^2\right\} M(k_x, k_y) \\ & \times \left\{ \sin k_x (x_p - x_m) \right\} \frac{dk_x dk_y}{k_z^*} \end{aligned} \tag{41}$$

The second integral is zero in all the integration domain, given that it is an odd sin() function. Therefore, we get

$$\begin{aligned} Y^*_{p,m} = {} & \frac{1}{4\pi^2 k\eta} \iint_{-\infty}^{+\infty} \left\{k_z^2 + |k_y|^2\right\} M(k_x, k_y) \\ & \times \left\{ \cos k_x (x_p - x_m) \right\} \frac{dk_x dk_y}{k_z^*} \end{aligned} \tag{42}$$

Given this simplification, we can focus on the first quadrant and solve the following integral

$$\begin{aligned} Y^*_{p,m} = {} & \frac{1}{4\pi^2 k\eta} \iint_{0}^{+\infty} \left\{k_z^2 + |k_y|^2\right\} M(k_x, k_y) \\ & \times \left\{ \cos k_x (x_p - x_m) \right\} \frac{dk_x dk_y}{k_z^*} \end{aligned} \tag{43}$$

The integral can be further decomposed in three terms

$$\begin{aligned} Y^*_{p,m} = {} & \frac{1}{4\pi^2 k\eta} \int_0^k \int_0^{\sqrt{k^2-k_x^2}} (k^2 - k_y^2) M(k_x, k_y) \\ & \times \left\{ \cos k_x (x_p - x_m) \right\} \frac{dk_x dk_y}{\sqrt{k^2 - k_x^2 - k_y^2}} + \\ & j \int_{-\infty}^k \int_{\sqrt{k^2-k_x^2}}^{-\infty} (k^2 - k_x^2) M(k_x, k_y) \\ & \times \left\{ \cos k_x (x_p - x_m) \right\} \frac{dk_x dk_y}{\sqrt{k^2 - k_x^2 - k_y^2}} \\ & + \int_k^{+\infty} \int_0^{+\infty} (k^2 - k_x^2) M(k_x, k_y) \\ & \times \left\{ \cos k_x (x_p - x_m) \right\} \frac{dk_x dk_y}{\sqrt{k^2 - k_x^2 - k_y^2}} \end{aligned} \tag{44}$$

Now, it is possible to easily separate the expression in its real part

$$\begin{aligned} R_e\{Y^*_{p,m}\} = {} & \frac{1}{\pi^2 k\eta} \int_0^k \int_0^{\sqrt{k^2-k_x^2}} (k^2 - k_y^2) M(k_x, k_y) \\ & \times \left\{ \cos k_x (x_p - x_m) \right\} \frac{dk_x dk_y}{\sqrt{k^2 - k_x^2 - k_y^2}} \end{aligned}$$

and imaginary part,

$$\begin{aligned} I_m\{Y^*_{p,m}\} = {} & \int_{-\infty}^k \int_{\sqrt{k^2-k_x^2}}^{-\infty} (k^2 - k_x^2) M(k_x, k_y) \\ & \times \left\{ \cos k_x (x_p - x_m) \right\} \frac{dk_x dk_y}{\sqrt{k^2 - k_x^2 - k_y^2}} \\ & + \int_k^{+\infty} \int_0^{+\infty} (k^2 - k_x^2) M(k_x, k_y) \\ & \times \left\{ \cos k_x (x_p - x_m) \right\} \frac{dk_x dk_y}{\sqrt{k^2 - k_x^2 - k_y^2}} \end{aligned} \tag{45}$$

The real part of the irradiation admittance can be solved in closed form by writing,

$$\begin{aligned} R_e\{Y^*_{p,m}\} = {} & \frac{T^2}{\pi^2 k\eta} \int_0^k (k^2 - k_y^2) \mathrm{sinc}^2 \left\{ \frac{T}{2} k_x \right\} \\ & \times \cos k_x (x_d) \left\{ \int_0^{\sqrt{k^2-k_x^2}} \mathrm{sinc}^2 \right. \\ & \left. \times \left(\frac{\Delta l}{2} k_y \right) \frac{dk_x dk_y}{\sqrt{k^2 - k_x^2 - k_y^2}} \right\} dk_x \end{aligned}$$

The integral in curly braces can be expanded as

$$\int_0^{\sqrt{k^2-k_x^2}} \mathrm{sinc}^2\Big(\frac{\Delta l}{2}k_y\Big)\frac{dk_x dk_y}{\sqrt{k^2-k_x^2-k_y^2}} = \frac{\pi}{(k^2-k_x^2)\Delta l^2}\sum_0^{+\infty}\frac{(-1)^n(\Delta l(k^2-k_x^2)^{2n+1})}{(2n+2)(2n+1)2^{2n}(n!)^2} \quad (46)$$

to get

$$R_e\{Y_{p,m}^*\} = \frac{T^2}{\pi^2 k\eta}\int_0^k (k^2-k_y^2)\mathrm{sinc}^2\Big(\frac{T}{2}k_x\Big) \times \frac{\pi}{(k^2-k_x^2)\Delta l^2}\sum_0^{+\infty}\frac{(-1)^n(\Delta l(k^2-k_x^2)^{2n+1})}{(2n+2)(2n+1)2^{2n}(n!)^2} \times \cos k_x(x_d)dk_x \quad (47)$$

This is the analytical expression which allows computing the real part of the admittance, which can be bound to be equal to the value of the feeding line.

As regards the imaginary part, Eq. 45 is made of three integrals, one of which is an improper integral, which nulls thanks to the odd sin() function. The integral can be simplified by using the relationships from Rhodes [46],

$$I_m\{Y_{p,m}^*\} = \frac{T^2}{\pi^2 k\eta}\int_0^k (k^2-k_y^2)\mathrm{sinc}^2\Big(\frac{T}{2}k_x\Big) \times \cos k_x(x_d)\Big\{\int_{\sqrt{k^2-k_x^2}}^{-\infty}\mathrm{sinc}^2\Big(\frac{\Delta l}{2}k_y\Big) \times \frac{dk_x dk_y}{\sqrt{k^2-k_x^2-k_y^2}}\Big\}dk_x + \frac{T^2}{\pi^2 k\eta} \times \int_k^{+\infty}(k^2-k_y^2)\mathrm{sinc}^2\Big(\frac{T}{2}k_x\Big)\cos k_x(x_d) \times \Big\{\int_0^{+\infty}\mathrm{sinc}^2\Big(\frac{\Delta l}{2}k_y\Big)\frac{dk_x dk_y}{\sqrt{k^2-k_x^2-k_y^2}}\Big\}dk_x \quad (48)$$

To speed up the computation of the imaginary part, the products in Eq. 21 are decomposed and solved separately.

ACKNOWLEDGMENT

The authors would like to sincerely thank Dr. Marco Simone for the irreplaceable and fruitful discussions which helped to improve this paper.

(Elena Marongiu and Alessandro Fanti contributed equally to this work.)

REFERENCES

[1] S. Raman, B. Graham, S. M. Crossan, N. Timmons, J. Morrison, V. A. Shameena, and M. Pezholil, "Microstrip fed ground modified compact antenna with reconfigurable radiation pattern for BANs," in *Proc. Loughborough Antennas Propag. Conf. (LAPC)*, Nov. 2012, pp. 1–4.

[2] S. M. Abbas, Y. Ranga, and K. P. Esselle, "Reconfigurable antenna options for 2.45/5 GHz wireless body area networks in healthcare applications," in *Proc. 37th Annu. Int. Conf. IEEE Eng. Med. Biol. Soc. (EMBC)*, Aug. 2015, pp. 5465–5468.

[3] F. Declercq, A. Georgiadis, and H. Rogier, "Wearable aperture-coupled shorted solar patch antenna for remote tracking and monitoring applications," in *Proc. 5th Eur. Conf. Antennas Propag. (EUCAP)*, Apr. 2011, pp. 2992–2996.

[4] S. Yan, P. J. Soh, and G. A. E. Vandenbosch, "Wearable dual-band magneto-electric dipole antenna for WBAN/WLAN applications," *IEEE Trans. Antennas Propag.*, vol. 63, no. 9, pp. 4165–4169, Sep. 2015.

[5] J. J. Heikkinen, T. T. Laine-Ma, and M. A. Kivikoski, "Flexible fabric-base patch antenna with protective coating," in *Proc. IEEE Antennas Propag. Soc. Int. Symp.*, Jun. 2007, pp. 4168–4171.

[6] R. M. Gonzalez, L. M. Peralta, and R. L. Y. Miranda, "Microstrip patch antenna array design for WLAN application," in *Proc. IEEE Int. Autumn Meeting Power, Electron. Comput. (ROPEC)*, Nov. 2015, pp. 1–5.

[7] K. Parashar and V. Singh, "Microstrip patch antenna for WiMAX/WLAN applications," *Advance Phys. Lett.*, vol. 1, pp. 34–37, May 2014.

[8] K. Noguchi, H. Rajagopalan, and Y. Rahmat-Samii, "Design of wideband/dual-band E-shaped patch antennas with the transmission line mode theory," *IEEE Trans. Antennas Propag.*, vol. 64, no. 4, pp. 1183–1192, Apr. 2016.

[9] G. Casu, C. Moraru, and A. Kovacs, "Design and implementation of microstrip patch antenna array," in *Proc. 10th Int. Conf. Commun. (COMM)*, May 2014, pp. 1–4.

[10] W. Zeng and J. Zhao, "A comb-shaped slot RFID tag antenna," in *Proc. IEEE Antennas Propag. Soc. Int. Symp.*, Jul. 2010, pp. 1–4.

[11] A. G. Markina, N. B. Pleshchinskii, and D. N. Tumakov, "On electrical characteristics of comb-shaped microstrip antennas," in *Proc. IEEE Conf. Russian Young Res. Electr. Electron. Eng. (EIConRus)*, Feb. 2017, pp. 179–183.

[12] J.-H. Lee, J. M. Lee, K. C. Hwang, D.-W. Seo, D. Shin, and C. Lee, "Capacitively coupled microstrip comb-line array antennas for millimeter-wave applications," *IEEE Antennas Wireless Propag. Lett.*, vol. 19, no. 8, pp. 1336–1339, Aug. 2020.

[13] K. S. R. Kumar, L. Prasad, B. R. Ramesh, K. P. Vinay, and R. P. Mallikarjuna, "Broad band com shaped microstrip patch antenna for X-band & Ku-band applications," *Amer. Int. J. Res. Sci., Technol., Eng. Math.*, vol. 23, no. 1, pp. 52–54, 2018.

[14] J. Jung, H. Lee, and Y. Lim, "Broadband flexible comb-shaped monopole antenna," *IET Microw., Antennas Propag.*, vol. 3, no. 2, pp. 325–332, Mar. 2009.

[15] B. Ramya, C. Supratha, and S. Robinson, "Design and analysis of comb shape microstrip patch array antenna for WLAN applications," *ICTACT J. Commun. Technol.*, vol. 9, no. 1, pp. 1702–1705, Mar. 2018.

[16] W. Zeng and J. Zhao, "A comb-shaped slot rfid tag antenna," in *Proc. IEEE Antennas Propag. Soc. Int. Symp.*, Jul. 2010, pp. 1–4.

[17] S. Afoakwa and Y.-B. Jung, "Wideband microstrip comb-line linear array antenna using stubbed-element technique for high sidelobe suppression," *IEEE Trans. Antennas Propag.*, vol. 65, no. 10, pp. 5190–5199, Oct. 2017.

[18] C.-C. Hsu, N.-C. Liu, S.-J. Wu, and J.-H. Tarng, "An ultra-wideband millimeter wave aperture-coupled patch antenna using a comb-shaped metasurface," in *Proc. IEEE Asia–Pacific Microw. Conf. (APMC)*, Dec. 2019, pp. 658–660.

[19] H. Baydar, M. Aslan, and V. T. Kilic, "Single and double side comb-shaped patch antenna design evolved from rectangular shape for reduced sized antenna applications," in *Proc. Int. Conf. Radar, Antenna, Microw., Electron., Telecommun. (ICRAMET)*, Nov. 2020, pp. 28–33.

[20] B. Majumder, K. Krishnamoorthy, and J. Mukherjee, "A novel compact comb shaped EBG structure for coupling reduction in Wimax band," in *Proc. IEEE Appl. Electromagn. Conf. (AEMC)*, Dec. 2013, pp. 1–2.

[21] K. Mandal, "Seven-band comb-shaped microstrip antenna for wireless systems," *Prog. Electromagn. Res. Lett.*, vol. 59, pp. 15–20, 2016.

[22] T. Kitazawa, "Variational method for multiconductor coupled striplines with stratified anisotropic media," *IEEE Trans. Microw. Theory Techn.*, vol. 37, no. 3, pp. 484–491, Mar. 1989.

[23] M. Matsunaga and K. Yasumoto, "Coupled-mode analysis of modal characteristic impedance of coupled bi-level microstrip lines," in *Proc. Asia–Pacific Microw. Conf.*, vol. 3, Dec. 1997, pp. 965–968.

[24] D. M. Pozar, "Microstrip antennas," *Proc. IEEE*, vol. 80, no. 1, pp. 79–91, Jan. 1992.

[25] M. L. Scarpello, I. Kazani, C. Hertleer, H. Rogier, and D. V. Ginste, "Stability and efficiency of screen-printed wearable and washable antennas," *IEEE Antennas Wireless Propag. Lett.*, vol. 11, pp. 838–841, 2012.

[26] A. Katyal and A. Basu, "Analysis and optimisation of broadband stacked microstrip antennas using transmission line model," *IET Microw., Antennas Propag.*, vol. 11, no. 1, pp. 81–91, Jan. 2017.

[27] F. Johansson, L. Rexberg, and N. Peterson, "Theoretical and experimental investigation of large Microstrip array antenna design," in *Proc. IEE Colloq. Recent Develop. Microstrip Antennas*, Feb. 1993, pp. 1–4.

[28] D. M. Pozar, S. Duffy, and N. Herscovici, "A comparison of commercial software packages for microstrip antenna analysis," in *IEEE Antennas Propag. Soc. Int. Symp. Transmitting Waves Prog. Next Millennium Dig. Held Conjunct: USNC/URSI Nat. Radio Sci. Meeting*, vol. 1, Jul. 2000, pp. 152–155.

[29] K. Esselle and A. K. Verma, "Fast and accurate model for circular microstrip antennas on suspended and composite substrates," *IEEE Trans. Antennas Propag.*, vol. 53, no. 9, pp. 3097–3100, Sep. 2005.

[30] M. Albani, G. L. Cono, R. Gardelli, and A. Freni, "An efficient full-wave method of moments analysis for RLSA antennas," *IEEE Trans. Antennas Propag.*, vol. 54, no. 8, pp. 2326–2336, Aug. 2006.

[31] K. Sankaran, "Are you using the right tools in computational electromagnetics?" *Eng. Rep.*, vol. 1, no. 3, 2019, Art. no. e12041.

[32] A. Fedeli, C. Montecucco, and G. L. Gragnani, "Open-source software for electromagnetic scattering simulation: The case of antenna design," *Electronics*, vol. 8, no. 12, p. 1506, Dec. 2019.

[33] S. Bedra, S. Benkouda, R. Bedra, and T. Fortaki, "Inverted HTS rectangular patch antennas: Theoretical investigation," *Phys. C, Supercond. Appl.*, vol. 580, Jan. 2021, Art. no. 1353802.

[34] M. A. Kolbehdari and M. N. O. Sadiku, "Finite and infinite element analysis of coupled cylindrical microstrip line in a nonhomogeneous dielectric media," in *Proc. IEEE Southeastcon Visualize Future*, Mar. 1995, pp. 269–273.

[35] I. Vilovic, N. Burum, and M. Brailo, "Microstrip antenna design using neural networks optimized by PSO," in *Proc. ICECom*, Oct. 2013, pp. 1–4.

[36] J. Wang, X.-S. Yang, and B.-Z. Wang, "Efficient gradient-based optimisation of pixel antenna with large-scale connections," *IET Microw., Antennas Propag.*, vol. 12, no. 3, pp. 385–389, 2017.

[37] R. Jian, Y. Chen, and T. Chen, "Multi-parameters unified-optimization for millimeter wave microstrip antenna based on ICACO," *IEEE Access*, vol. 7, pp. 53012–53017, 2019.

[38] Z. Zhang, H. C. Chen, and Q. S. Cheng, "Surrogate-assisted quasi-Newton enhanced global optimization of antennas based on a heuristic hypersphere sampling," *IEEE Trans. Antennas Propag.*, vol. 69, no. 5, pp. 2993–2998, May 2021.

[39] D. Chang, "Analytical theory of an unloaded rectangular microstrip patch,," *IEEE Trans. Antennas Propag.*, vol. 29, no. 1, pp. 54–62, Jan. 1981.

[40] C. Nucci, F. Rachidi, and M. Rubinstein, "Derivation of telegrapher's equations and field-to-transmission line interaction," in *Electromagnetic Field Interaction With Transmission Lines: From Classical Theory to HF Radiation Effects*, vol. 5. Southampton U.K.: WIT Press, 2008, p. 3.

[41] F. W. Grover, *Inductance Calculations: Working Formulas and Tables*. Chelmsford, MA, USA: Courier Corporation, 2004.

[42] X. Zhang, J. Fang, K. K. Mei, and Y. Liu, "Calculations of the dispersive characteristics of microstrips by the time-domain finite difference method," *IEEE Trans. Microw. Theory Techn.*, vol. 36, no. 2, pp. 263–267, Feb. 1988.

[43] K. Noguchi, S. Betsudan, S. Makino, T. Hirota, and K. Itoh, "Transmission line mode analysis of wideband/multiband antennas consisting of coupled conductors," in *Proc. IEEE-APS Top. Conf. Antennas Propag. Wireless Commun. (APWC)*, Sep. 2013, pp. 272–275.

[44] Y. Hao and R. Mittra, *FDTD Modeling of Metamaterials: Theory and Applications*. Norwood, MA, USA: Artech House, 2008.

[45] S. D. Gedney, "Introduction to the finite-difference time-domain (FDTD) method for electromagnetics," *Synth. Lectures Comput. Electromagn.*, vol. 6, no. 1, pp. 1–250, Jan. 2011.

[46] D. R. Rhodes, "On a fundamental principle in the theory of planar antennas," *Proc. IEEE*, vol. 52, no. 9, pp. 1013–1021, Sep. 1964.

[47] C. Chhabra, "Improvements in the bisection method of finding roots of an equation," in *Proc. IEEE Int. Advance Comput. Conf. (IACC)*, Feb. 2014, pp. 11–16.

[48] A. C. Newell and D. M. Kerns, "Determination of both polarisation and power gain of antennas by a generalised 3-antenna measurement method," *Electron. Lett.*, vol. 7, no. 3, pp. 68–70, Feb. 1971.

[49] R. K. Kanth, Q. Wan, H. Kumar, P. Liljeberg, Q. Chen, L. Zheng, and H. Tenhunen, "Evaluating sustainability, environment assessment and toxic emissions in life cycle stages of printed antenna," *Proc. Eng.*, vol. 30, pp. 508–513, Jan. 2012.

[50] I. Locher, M. Klemm, T. Kirstein, and G. Trster, "Design and characterization of purely textile patch antennas," *IEEE Trans. Adv. Packag.*, vol. 29, no. 4, pp. 777–788, Nov. 2006.

[51] Y. Ouyang and W. J. Chappell, "High frequency properties of electro-textiles for wearable antenna applications," *IEEE Trans. Antennas Propag.*, vol. 56, no. 2, pp. 381–389, Feb. 2008.

[52] G. Kim, J. Lee, K. Hwan Lee, Y. Chung Chung, J. Yeo, B. Hyun Moon, J. Yang, and H. Cheol Kim, "Design of a UHF RFID fiber tag antenna with electric-thread using a sewing machine," in *Proc. Asia–Pacific Microw. Conf.*, Dec. 2008, pp. 1–4.

[53] P. Salonen, Y. Rahmat-Samii, M. Schaffrath, and M. Kivikoski, "Effect of textile materials on wearable antenna performance: A case study of GPS antennas," in *Proc. IEEE Antennas Propag. Soc. Symp.*, vol. 1, Jun. 2004, pp. 459–462, 2004.

[54] L. Vallozzi, W. Vandendriessche, H. Rogier, C. Hertleer, and M. L. Scarpello, "Wearable textile GPS antenna for integration in protective garments," in *Proc. 4th Eur. Conf. Antennas Propag.*, Apr. 2010, pp. 1–4.

ELENA MARONGIU received the bachelor's degree in electrical and electronic engineering, in 2016, and the master's degree in telecommunications engineering, in 2019. She is currently pursuing the Ph.D. degree in electronic engineering and computer science with the University of Cagliari. Her research interests include modeling, design, and characterization of antennas, and in the development of microwave devices and components for radio-astronomical applications, especially for both near and deep space in K- and X-bands.

ALESSANDRO FANTI (Member, IEEE) received the Laurea degree in electronic engineering and the Ph.D. degree in electronic engineering and computer science from the University of Cagliari, Cagliari, Italy, in 2006 and 2012, respectively. He worked as a Postdoctoral Fellow with the Electromagnetic Group, University of Cagliari, from 2013 to 2016, where he is currently an Assistant Professor. He has coauthored more than 100 scientific contributions published in international journals, conference proceedings, and book chapters. His research interests include the use of numerical techniques for modes computation of guiding structures, optimization techniques, analysis, and design of waveguide slot arrays, analysis, and design of patch antennas, radio propagation in urban environment, modeling of bio-electromagnetic phenomena, and microwave exposure systems for biotechnology and bio-agriculture. He is a member of the IEEE Antennas and Propagation Society, the Italian Society of Electromagnetism, and the Interuniversity Center for the Interaction Between Electromagnetic Fields and Biosystems. Since 2020, he has been acting as a Principal Investigator of the IAPC Project, funded with five million euros by the Italian Ministry of Economic Development (MISE), within the AGRIFOOD PON I&C (2014–2020). He is also an Associate Editor of the IEEE JOURNAL OF ELECTROMAGNETICS, RF AND MICROWAVES IN MEDICINE AND BIOLOGY.

SANTI CONCETTO PAVONE (Senior Member, IEEE) was born in Patti (ME), Italy, in 1988. He received the B.Sc. and M.Sc. degrees *(summa cum laude)* in electronics engineering from the University of Messina, Messina, Italy, in 2010 and 2012, respectively, and the Ph.D. degree (with the additional label of ''Doctor Europaeus'') in information engineering and science (electromagnetics engineering) from the University of Siena, Siena, Italy, in 2015.

He was a Visiting Ph.D. Student with the Institut d'Electronique et de Telecommunications de Rennes (IETR), Université de Rennes 1, Rennes, France, for five months, in 2015. From 2016 to July 2019, he was an Associate Researcher with the Laboratory of Applied Electromagnetics, University of Siena. Since August 2019, he has been an Assistant Professor with the Department of Electrical, Electronics, and Information Engineering (DIEEI), University of Catania, Catania, Italy. His current research interests include fundamental electromagnetic theory, radar design at millimeter waves, high-frequency techniques, focusing systems, nondiffractive localized pulses, and leaky-wave reconfigurable antennas based on liquid crystals.

Dr. Pavone was a recipient of the European Science Foundation (ESF) Research Networking Programme NEWFOCUS Scholarship, in 2015, and the IEEE Antennas and Propagation Society Student Award, Chapter of the Central-Southern Italy, in 2014. In 2017, he was a Finalist of the Best Paper Award in Electromagnetics and Antenna Theory at the 11th European Conference on Antennas and Propagation, Paris. In 2018, he was a co-recipient of the Best Paper Award in Electromagnetics and Antenna Theory at the 12th European Conference on Antennas and Propagation, London, U.K. In 2019, he was also a recipient of the Young Scientist Award (YSA) at the 41st Progress in the Electromagnetics Research Symposium (PIERS 2019), Rome, Italy. He serves as an Associate Editor for IEEE Access and a reviewer for the IEEE Transactions on Antennas and Propagation.

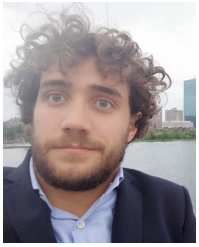

MATTEO BRUNO LODI (Graduate Student Member, IEEE) received the bachelor's degree in biomedical engineering from the University of Cagliari, Cagliari, in 2016, and the master's degree in biomedical engineering from the Politecnico di Torino, Turin, Italy, in 2018. He is currently pursuing the Ph.D. degree in electronic engineering and computer science with the University of Cagliari. His research interests include modeling of bioelectromagnetic phenomena, especially hyperthermia treatment; the study, manufacturing, and synthesis of magnetic biomaterials for tissue engineering applications; and the use of microwave for biotechnology and environmental applications. He was awarded as the Young Scientists at General Assembly and Scientific Symposium of URSI (2020 and 2021). He has been appointed as the Representative for the Young Professionals of IEEE Region 8 for the Nanotechnology Council. He is a member of the Editorial Board of *IEEE Future Directions Technology Policy and Ethics Newsletter*.

ANDREA MELIS received the bachelor's degree in biomedical engineering from the University of Cagliari, Italy, in 2017. He worked as an Assistant Researcher with the University of Cagliari. His research interests include EM modeling and development of RF coils at low and high frequencies, especially for MRI at high field, the design and realization of WSN systems for the monitoring of industrial processes, such as bread manufacturing, and intelligent transportation systems.

NICOLA CURRELI received the M.Sc. degree from the University of Genoa, Genoa, Italy, in 2016, and the Ph.D. degree in electronic engineering from the University of Cagliari, Cagliari, Italy, and the Italian Institute of Technology—IIT, Genoa, in 2020. After the Ph.D. degree, he held a fellow position at Graphene Labs—IIT in the WP12 (Energy storage) of the Graphene Core 2 Project (graphene flagship). In 2019, he was a Visiting Researcher with the Physics and Mechanical Engineering Department, Columbia University, New York City, NY, USA. He is currently a Postdoctoral Researcher at the Functional Nanosystems Group. His research interests include the study of low-dimensional materials, their characterization, and their application in the field of photonics, as well as the design, implementation, and analysis of linear and nonlinear integrated optical, microwave devices, and antennas.

CLAUDIA MUSU received the master's degree in telecommunication and the Ph.D. degree in electronic engineering and computer science from the University of Cagliari, Cagliari, Italy, in 2009 and 2015, respectively. Her main research interests include body area networks, microwave antennas, object detection, real-time systems, risk analysis, and risk management.

GINO SORBELLO received the Laurea degree in electronics engineering *(cum laude)* from the University of Catania, Catania, Italy, in 1996, and the Ph.D. degree in electronics and communications engineering from the Polytechnic Institute of Milan, Milan, Italy, in 2000. He became an Assistant Professor of electromagnetic fields with the University of Catania, in 2002. Since 2014, he has been an Associate Professor of electromagnetic fields with the Department of Electric, Electronics, and Computer Engineering, University of Catania. Since 2012, he has been a member of INFN-LNS and collaborates with the Ion Sources and Plasma Physics Group. His current research interests include single-mode solid-state waveguide lasers and amplifiers, integrated optics, development of planar antennas and ultra-wideband compact antennas, and the study of microwave devices and computational electromagnetism with a special interest in RF–plasma interactions and particle accelerators.

GIUSEPPE MAZZARELLA (Senior Member, IEEE) received the degree *(summa cum laude)* in electronic engineering from the Università Federico II of Naples, in 1984, and the Ph.D. degree in electronic engineering and computer science, in 1989. In 1990, he became an Assistant Professor at the Dipartimento di Ingegneria Elettronica, Università Federico II of Naples. Since 1992, he has been with the Dipartimento di Ingegneria Elettrica ed Elettronica, Università di Cagliari, first as an Associate Professor and then, since 2000, as a Full Professor, teaching courses in electromagnetics, microwave, antennas and remote sensing. He is the author (or coauthor) of over 70 articles in international journals and a reviewer for many EM journals. His research interests include the efficient design of large arrays of slots, power synthesis of array factor, with emphasis on inclusion of constraints, microwave holography techniques for the diagnosis of large reflector antennas, use of evolutionary programming for the solution of inverse problems, in particular problems of synthesis of antennas and periodic structures.